PROCEEDINGS, 41st Workshop on Geothermal Reservoir Engineering
Stanford University, Stanford, California, February 22-24, 2016
SGP-TR-209

Fluid Imaging, Moment Tensors and Finite Source Models During the EGS Demonstration Project at The Geysers, CA

Roland Gritto[1], Douglas S. Dreger[2], O. Sierra Boyd[2], and Taka'aki Taira[2]

[1]Array Information Technology, Berkeley, CA 94709, [2]Berkeley Seismological Laboratory, UC, Berkeley, CA 94720
roland.gritto@arrayinfotech.com, ddreger@berkeley.edu

Keywords: Moment Tensor, Finite-Source, Vp/Vs Ratio

ABSTRACT

We investigate seismicity in the vicinity of the EGS development at The Geysers Prati-32 injection well. The goals of our study include the ability to estimate the activated fracture area and volume, to estimate stress drop and stress drop changes as well as fluid saturation and temporal changes in fluid distribution. For this paper we have incorporated the capability of simultaneously inverting full waveform data and P-wave polarities to improve estimates of the source mechanism of small events. We have analyzed the full moment tensor of more than 80 events (M>~1.0) using a semi-automated approach, and have investigated finite-source models of five Geysers events ranging in magnitude from M 3.7 to 4.5. We find that combination of first-motion and waveforms from the Lawrence Berkeley National Laboratory (LBNL) network results in solutions for some events having positive isotropic or volume increase components. Other events appear to be predominantly double-couples. Ongoing work is examining the temporal evolution of the moment tensors during the injection process. The finite-source scaling relationship between rupture area and moment magnitude, found for the investigated events at The Geysers, resembles that of a published empirical relationship derived for field and aftershock data for events from M 4.5 to 8.3. In order to perform temporal analysis of the subsurface water saturation, we compiled and analyzed seismicity catalogs recorded by the LBNL seismic network for the area around the EGS development project. The data are analyzed using the double-difference Wadati method.

1. INTRODUCTION

Identifying, creating, and managing fractures and flow paths are essential tasks during EGS resource development. The successful generation of a fracture network requires a priori knowledge of in-situ stress and natural fracture orientation and spacing, among others. However, because the orientation and magnitude of in-situ stress may not be reliably available and injecting fluids at high rates and volume may disturb the natural stress state, it is advantageous to monitor in-situ stress during the injection process. Knowing the stress evolution, the size of the fractures and the speed of the rupture process, as well as the spatial distribution and the velocity of the fluid flow are essential to control the generation of the fracture network. Our ongoing research addresses these issues by developing an integrated technology approach, to estimate in-situ stress, size of the generated fractures, fluid migration velocity, and spatio-temporal fluid distribution during reservoir stimulation.

Our research goal is to improve technology to assess in-situ stress magnitude and orientation, kinematic fracture parameter, rupture size, as well as temporal and volumetric distribution of the injected fluid during Enhanced Geothermal System (EGS) resource development. We leverage high-frequency seismic data recorded by the LBNL 34-station permanent geophone network and seismic broadband data recorded by a temporary 33-station seismometer network that operated in The Geysers during the injection phase of the DOE GTO funded EGS demonstration project at Prati-32. The operation of the broadband network with high station density and azimuthal coverage to monitor the injection phase produced an unprecedented dataset that is typically unavailable for EGS operations. The two datasets offer two main advantages. (1) The parameters under investigation can be studied over a broader frequency band and at distinct sensitivity levels and (2) the higher sensitivity of the broadband seismometers resulted in a richer dataset with a lower magnitude of completeness.

A first step for both inverting for in situ stress and for developing a source-area scaling relationship is the development of a robust seismic moment tensor catalog. Using waveform data from the LBNL short-period network we have refined a semi-automated approach for estimating the seismic moment tensor and have applied the method to more than 80 M>1.0 events. In parallel we have also begun to search for suitable target and empirical Green's function event pairs to determine seismic moment rate functions and to use those moment rate functions to determine finite-source parameters. For the estimation of fluid saturation we evaluated two approaches, based on the double-difference Wadati method and tested several fitting methods to account for uncertainty in differential waveform arrivals and outliers in the resulting data. We also compiled seismicity catalogues from the LBNL database and analyzed the data for differential travel times. In the following, the preliminary of our study are discussed.

2. TECHNICAL RESULTS

2.1 Seismic Moment Tensor Inversion

We have been investigating seismic moment tensor solutions for micro earthquakes associated with the Prati-32 Enhanced Geothermal System (EGS) stimulation experiment. Figure 1 shows the study area, with the locations of the Prati-32 injection well and nearby stations. We have defined the rectangular region as our study area to investigate the seismicity in detail, applying waveform modeling and inversion methods to obtain seismic moment tensor parameters. Towards this goal we have evaluated the three-component waveform data recorded by the LBNL short-period Geysers network and have found the data to be of very high quality, suitable for waveform inversion for seismic source parameters. The challenge is that given the large numbers of small events occurring in response to fluid injection the usual approaches employed needed to be streamlined and partially automated.

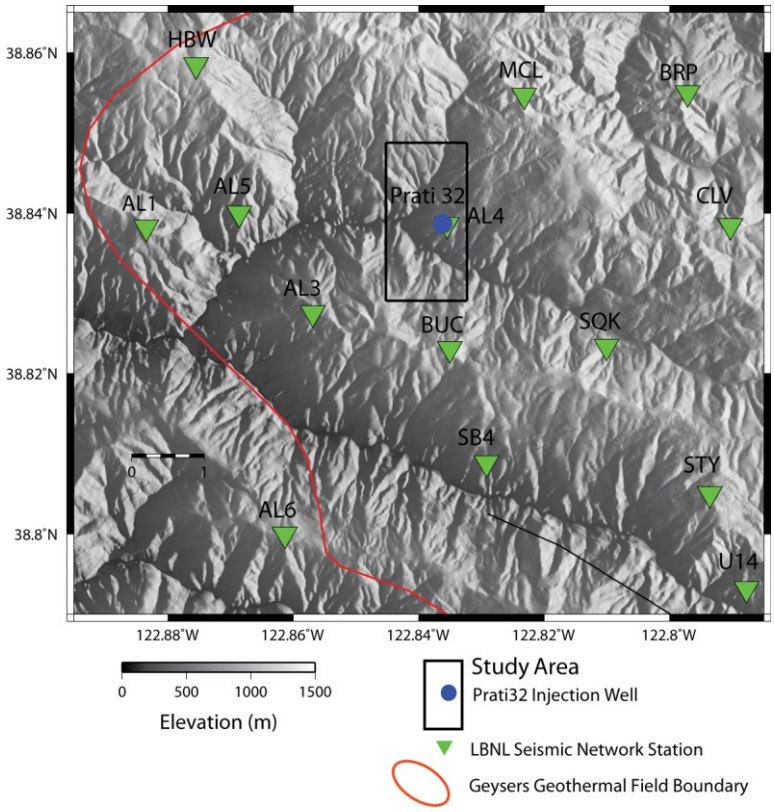

Figure 1: Map of the Northwest Geysers geothermal field. The EGS Development study area denoted by the rectangle encloses the EGS production well Prati-31 (P-31) and the EGS injection well Prati-32 (P-32, blue dot). Short-period seismic stations operated by LBNL used in this study are denoted by inverted green triangles. The boundary of The Geysers geothermal field and selected faults are delineated with red and black lines, respectively.

The LBNL seismic network currently consists of 34 three-component short-period (4.5 Hz) geophones sampled at 500 Hz (Majer and Peterson, 2007). A subset of seismic stations used in this study is shown in Figure 1. Earthquakes with magnitude $M \geq 1$ were chosen for deviatoric moment tensor investigation. Events are located to within 100 m accuracy (Majer and Peterson, 2007). For the largest earthquake, Mw 3.74, the moment tensor solution was determined using the Berkeley Seismological Laboratory (BSL) moment tensor interface and broadband data from the Berkeley Digital Seismic Network (BDSN). Data for the $1.0 \leq M \leq 3.7$ events are obtained from the local LBNL short-period seismic network. The seismic waveform data are processed by removing the instrument response to ground velocity followed by bandpass filtering of the waveforms with a causal 4th-order Butterworth filter with corners at 0.7 and 1.7 Hz (0.6 to 1.4 s period) for $1 \leq M < 2.8$ events and 0.2 and 1.0 Hz for $M \geq 2.8$ events. The data are subsequently resampled at 0.1 s.

Synthetic Green's functions for the inversion are computed using a 1-D velocity model, derived from a 3-D velocity model for the Northwest Geysers developed by Julian et al. (1996). This model was shown to perform well for moment tensor inversion (e.g. Guilhem et al., 2014). The synthetic Green's functions, including near-, intermediate-, and far-field terms for body and surfaces waves, are computed using Computer Programs in Seismology, Herrmann (2013). Our analysis is restrained to event depths reported in the DOE Geysers EGS catalog or when necessary the NCSS catalog.

Seismic moment tensors are computed utilizing the methods described in Minson and Dreger (2008), Ford et al. (2010) and Boyd et al., (2015). Part of this analysis requires the alignment of the observed waveforms to the computed Green's functions. With a well calibrated velocity model it is sometimes possible to invert the waveform data without timing shifts, however in our analysis data time shifting is necessary, and the shifts represent departures from the assumed velocity model with the actual velocity structure along the

paths. Typically the time shifts are estimated by trial and error, however due to the large numbers of events investigated we employed a grid search to find the best time alignment shifts automatically. The results of the time shift analysis are presented below.

An effort was made to have as many stations in common as possible for all of the studied events. Initially seismic data from as many as 10 stations within 6 km of the studied events were considered for preliminary moment tensor analysis. Depending on these initial fits of the observed data with the synthetic Green's functions, 5-6 stations were selected for moment tensor processing using a grid-search algorithm to automatically find the optimal alignment of the observed data with the synthetic Green's functions. This method is applied to all of the studied events for automated moment tensor computation. These results are then checked and if necessary minor adjustments are applied to shift the data for optimal fit. In the final processing stage, data with poor fit are removed.

The alignment results are presented as a histogram in Figure 2. Zero indicates no shift and the consistency between the catalog origin time and the theoretical arrival time of the wave packet with respect to the velocity model that has been employed to compute the synthetic Green's functions. The results indicate a systematic shift to negative zcor values with the mean at approximately -3 samples or -0.3 seconds. This indicates that the data need to be shifted to a later time indicating that the model is slower on average than the actual Earth structure. The magnitude of the shifts on average are approximately 1/3 of the central period of the utilized passband. The mean shift value does not appear to change during injection.

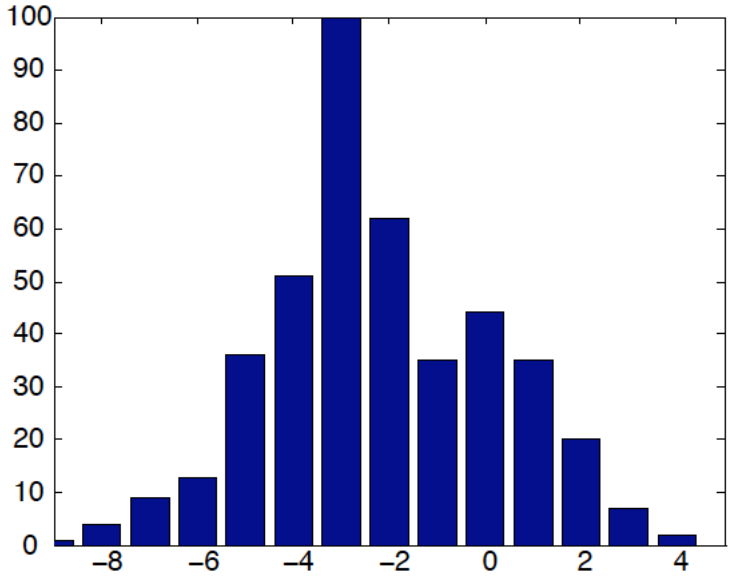

Figure 2: Distribution of alignment parameter, zcor (sample shift) for all studied events. The time shift in seconds is found by multiplying by the sample interval of 0.1 seconds/sample.

Thus far, solutions for more than 80 events have been obtained. Figure 3 shows the focal mechanisms (deviatoric moment tensor solutions) of a subset of the injection events. Reservoir stimulation at Prati-32 began on October 6, 2011, was temporarily halted in late August 2012 for a period of 160 days, before it recommenced in early February 2013. There are two dominant classes of earthquakes, those with predominantly strike-slip mechanisms and those with normal mechanisms. These mechanisms are consistent with what we have found previously in other regions of The Geysers (Guilhem et al., 2014; Boyd et al., 2015). Within these two broad populations there is fairly large variability in the focal parameters.

We have reviewed the uncertainties in the strike, dip and rake focal parameters as well as the scalar seismic moment by performing Jackknife tests, in which multiple inversions are performed omitting one of the recording stations. We consider all permutations of minus-1 station cases. Figure 4a is an example of this analysis for a Mw 1.9 event that occurred on March 27, 2012 during the injection period. The waveform fits for the six used stations are good, and the azimuthal coverage indicates that the solution should be well constrained. The Jackknife test reveals that the uncertainties in the strike/dip/rake focal parameters is 8/2/13 degrees, respectively, and that the uncertainty in scalar seismic moment is only 5%. The uncertainties for other events are comparable.

The Jackknife test for the March 27, 2012 event consistently recovered a large CLVD component where the average percent CLVD was 80% ±5% of the total scalar moment. It is also interesting that when the full moment tensor is solved for (Figure 4b) a large positive isotropic component is found. The F-test for the extra degree of freedom is only significant at 55%, and therefore based on that measure alone we would not be confident in the isotropic component. It is interesting, however, that when the first-motion polarities are considered for this event they are more consistent with the full moment tensor result. Using the NSSinv method of Nayak and Dreger (2015) we simultaneously inverted the waveform data and first-motion polarities and found the solution shown in Figure 5. This solution reveals a relatively large isotropic component, which appears to be required by the first-motion polarity data. This interesting result warrants further analysis, and it will be an objective to find other events in our moment tensor catalog that may have significant volumetric components in their moment tensor solutions. The goal will be to determine if resolved isotropic components change over time during the stimulation experiment.

The Mw 2.87 event on February 6, 2013 on the other hand shows a large double-couple solution (Figure 6), and similarly when the full moment tensor solution is solved for, the percent double-couple remains a dominant 62%. The NSSinv joint inversion of waveform and first-motion data recovers a solution that is dominantly double-couple with a small, statistically insignificant volume decrease component (Figure 7). In Figure 7b it can seen that the small volume decrease comes from fitting a single dilational P-wave observation on the west side of the focal sphere. Our interpretation for this event is that of a double-couple.

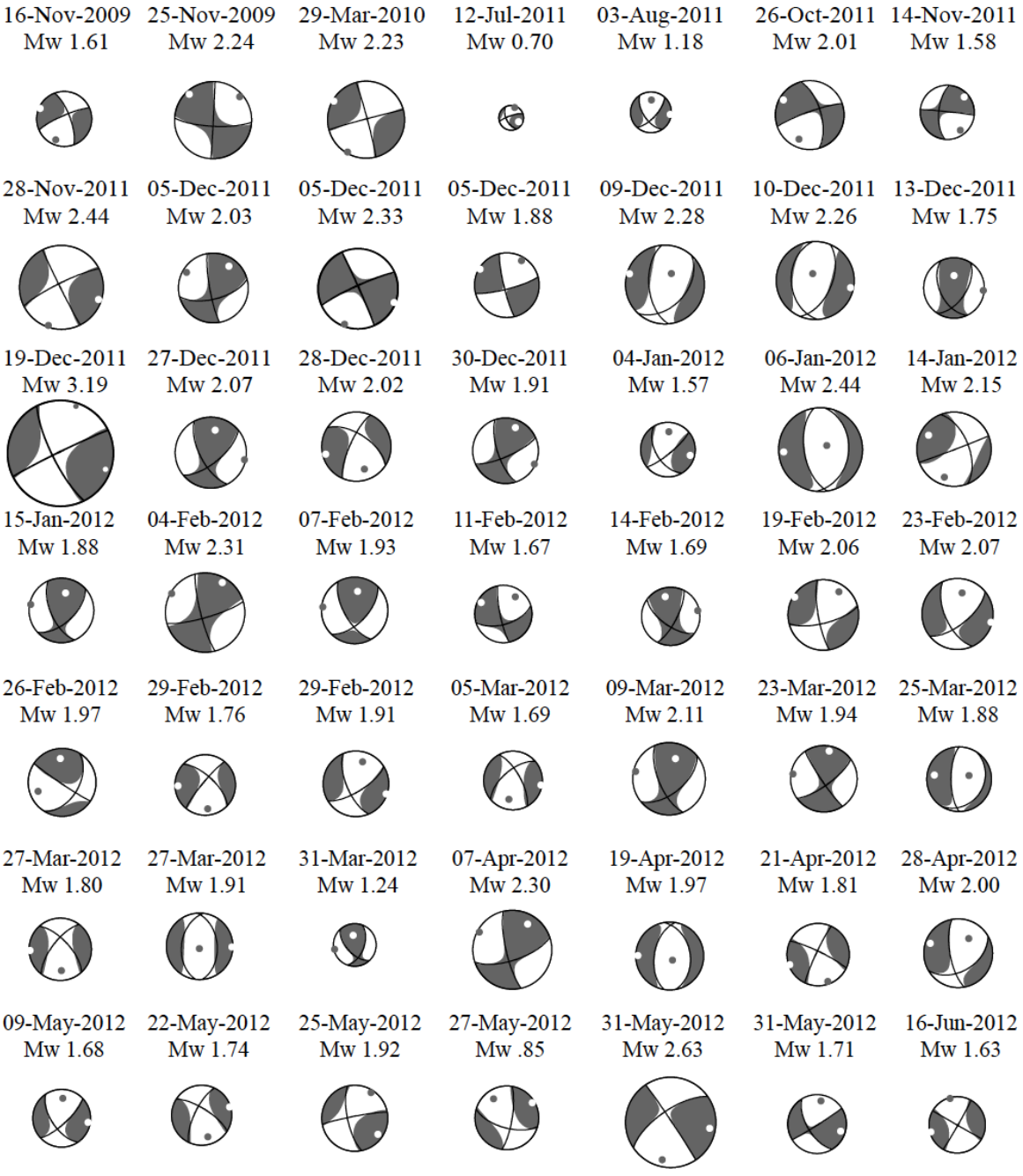

Figure 3: Time-sequential deviatoric moment tensor solutions. Gray and white dots represent, respectively, pressure and tension axes. The reservoir stimulation at Prati-32 began on October 6, 2011, and was temporarily halted late August 2012 for a period of 160 days and recommenced in early February 2013.

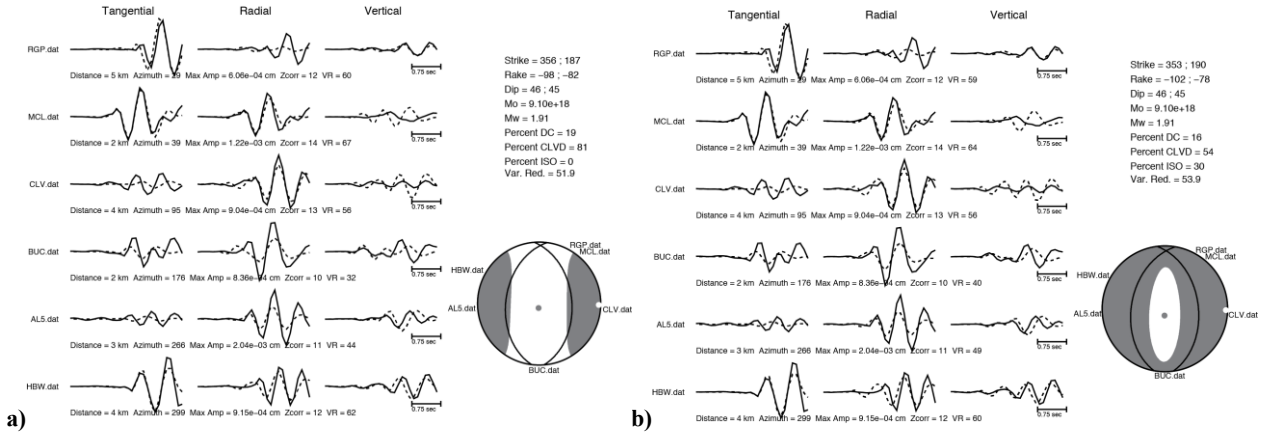

Figure 4: a) Deviatoric moment tensor solution for the Mw 1.9 event on March 27, 2012. b) Full moment tensor solution for the event in a). Gray and white dots represent, respectively, pressure and tension axes.

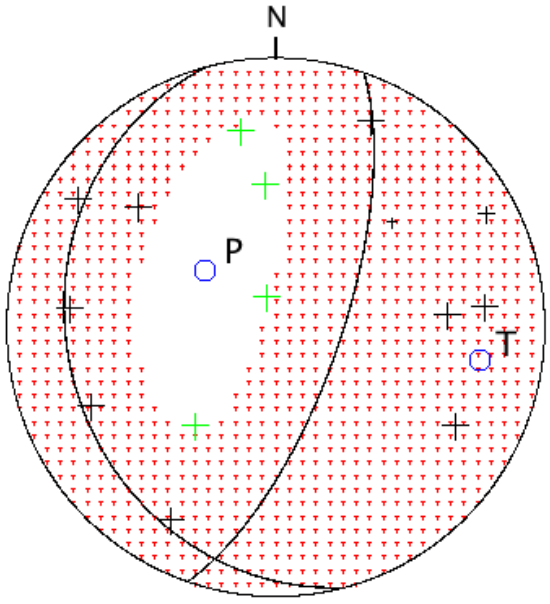

Figure 5: Comparison of observed first-motion polarity (black and green crosses denote, respectively, first motion up and down) with the moment tensor solution obtained by jointly inverting the waveform data shown in Figure 4 and the first-motion polarities.

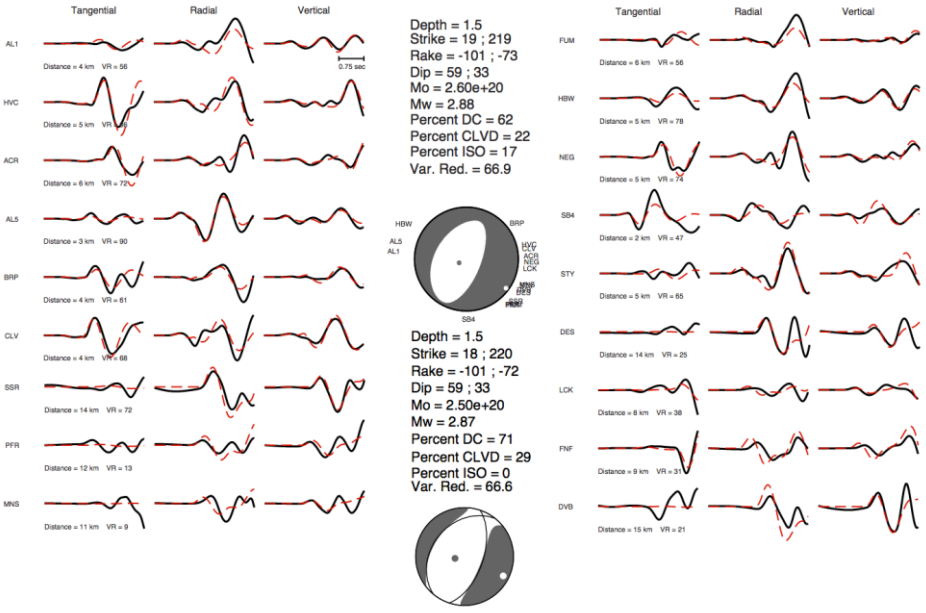

Figure 6: Comparison of filtered (0.2 to 1.0 Hz) observed velocity data (black) and synthetics (red) waveform fits and P-wave radiation pattern of the full moment tensor solution (upper focal mechanism) and deviatoric moment tensor solution (lower focal mechanism) for event 60, a Mw 2.87 on 6 February 2013. The improvement in fit of the full moment tensor solution is 0.3% and is too small to be statistically significant. Gray and white dots represent, respectively, pressure and tension axes.

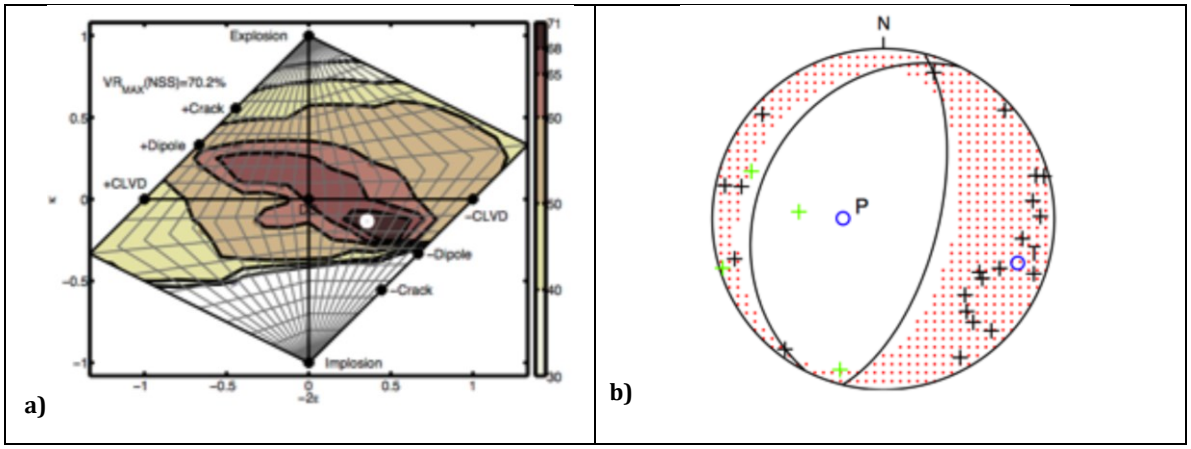

Figure 7: a) NSSinv result for the February 6, 2013 event. The white circle shows the best fitting solution. b) The distribution of the goodness of fit parameter shows a distribution that can include a double-couple mechanism. Black and green crosses denote, respectively, first motion up and down.

2.2 Finite-Source Inversion

Given a moment tensor solution, it is possible to test which of the two possible nodal (fault) planes is the causative plane. For small events related to the EGS stimulation project it is necessary to consider higher frequencies and therefore the use of theoretical Green's functions based on simple plane layered velocity models is not adequate. Therefore empirical Green's functions are derived, utilizing the waveforms of nearly collocated smaller events. Mori (1993) demonstrated that the waveform of a smaller earthquake could be spectrally deconvolved from the larger target earthquake yielding an estimate of the seismic moment rate function (MRF). Several MRF observed at different seismic stations can subsequently be inverted for fault slip, as well as to identify the causative rupture plane.

Dreger et al. (2007) applied this approach at Parkfield, California, and found that it is possible to obtain finite-source parameters for micro-earthquakes exhibiting rupture complexity, and kinematic parameters that are comparable to their larger counterparts.

Figure 8 shows the slip distribution of the Mw 3.7 event (Figure 3) obtained by deconvolving the records of a nearby Mw 2.5 earthquake. The slip distribution is complex, with 3 or 4 asperities being well resolved. The moment rate functions show multiple pulses of moment release that give rise to the observed slip patches. The average and peak slips are 4.3 and 26.6 cm, respectively. Using the method of Ripperger and Mai (2004) the slip distribution can be mapped into stress change. The average stress drop over the fault rupture is 11 MPa, with a peak stress drop of 68 MPa. These high stress drops result from the compact nature of the individual slip patches in the rupture model, and demonstrate that the field is under high stress.

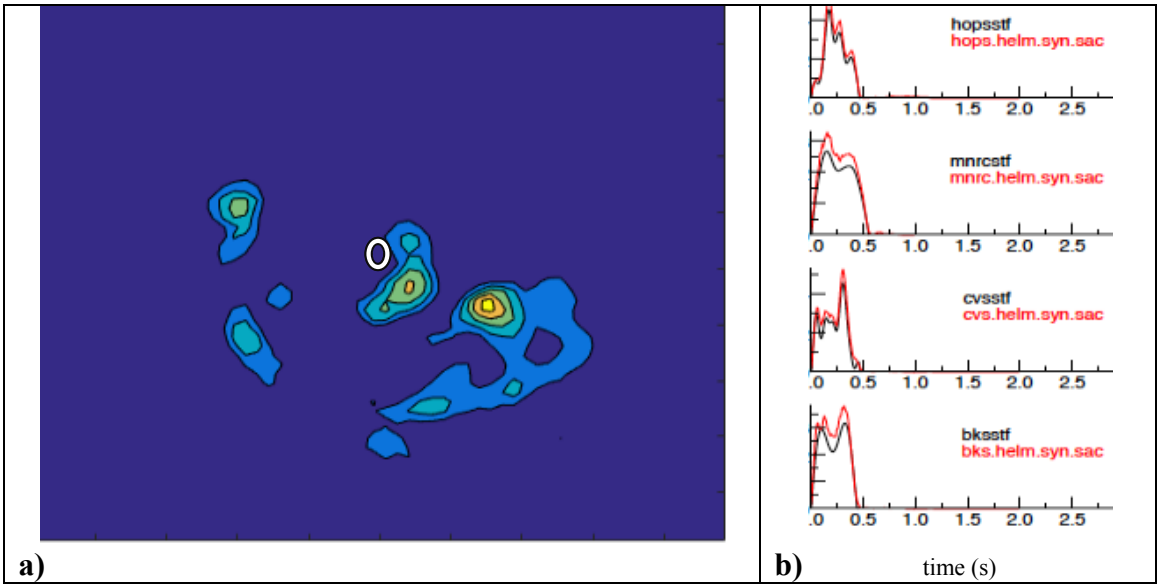

Figure 8: a) Slip distribution for the January 21, 2014 Mw 3.7 event. The hypocenter is indicated by the white ellipse. b) Observed moment rate functions (black) are compared to synthetics at the four stations, HOPS, MNRC, CVS and BKS. The amplitudes are proportional to 7.5e19 dyne cm/s.

Thus far we have analyzed the finite-source models of five Geysers events ranging in magnitude from 3.7 to 4.5. One objective of our research is to estimate the coseismic fracture density of the EGS seismicity cloud. This will be achieved by first determining moment tensor solutions to obtain focal mechanisms and robust magnitude estimates. Second, suitable target EGF event pairs are found to obtain MRF, which are subsequently inverted for fault slip and the orientation of the causative fault plane. Stress change maps using the method of Ripperger and Mai (2004) may then be determined. Once slip models are available for a number of events over a range of magnitude, the scaling relationship between rupture area and magnitude can be determined.

Figure 9 shows the scaling of rupture area as a function of magnitude for the five events that we have studied. The data are compared to the empirical area-magnitude scaling relationship of Wells and Coppersmith (1994), which is based on field and aftershock data for events from M 4.5 to 8.3, where the majority of events are in the M 6-7 range. The comparison is very good, considering the substantial extrapolation to lower magnitudes. Nevertheless, the extrapolated relationship is consistent with the rupture area estimates obtained for the five Geysers earthquakes. It appears that four of the five events are collinear. The average stress drops of these events are between 6 and 17 MPa. The largest event (Mw 4.5), which occurred on January 12, 2014, had an average stress drop of 1.6 MPa. Judging from Figure 9, the relatively low stress drop Mw 4.5 event may be more consistent with the Wells and Coppersmith (1994) scaling relationship, although there are presently too few points to be able to reach reasonable conclusions. We have begun searching for suitable EGF target event pairs using the LBNL network data. In Figure 10 we show seismic moment rate functions obtained for the Mw 2.87 February 6, 2013 event (Figures 3, 6 and 7) using the waveforms from a nearby M1.4 event as the EGF. Very preliminary finite-source inversions reveal a rupture area of approximately 0.05 km^2, which is consistent with the results shown in Figure 9 in that scaling at The Geysers is found to have a slope similar to the Wells and Coppersmith (1994) relationship, but tend to plot below the relationship. With additional finite-source information we will be able to calibrate a rupture-area/Mw scaling relationship for The Geysers.

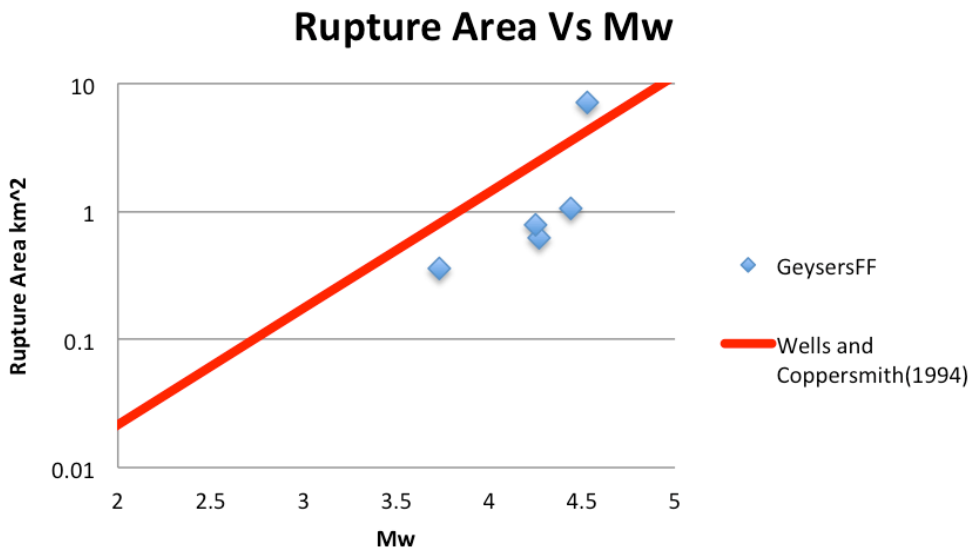

Figure 9: Relationship between finite-source rupture area and Mw. The diamonds represent the relationship between rupture area and magnitude Mw, as inferred from slip models from finite-source inversion. The red line is an extrapolation of the Wells and Coppersmith (1994) empirical relationship based on field observations of large earthquakes.

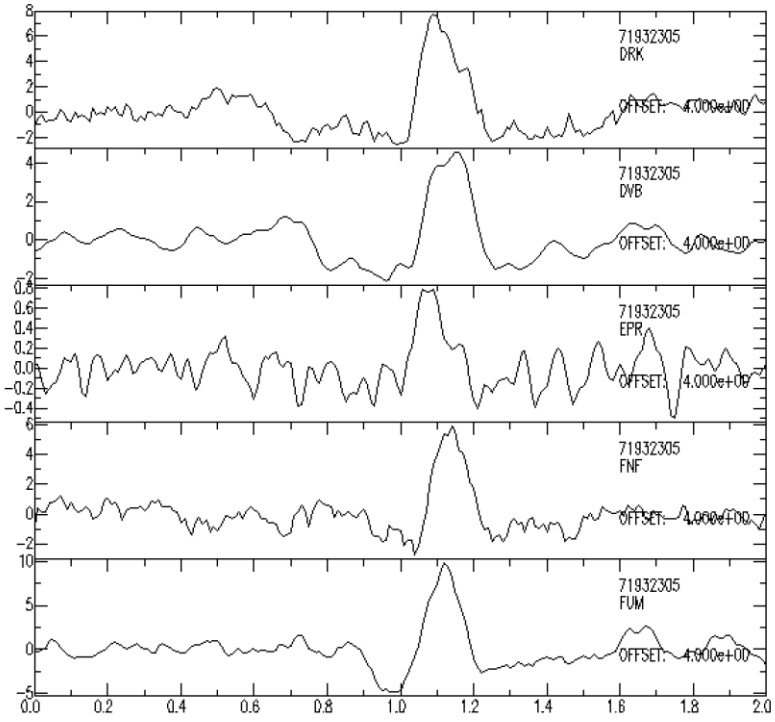

Figure 10: Seismic moment rate functions for the Mw 2.87 February 6, 2013 event from empirical Green's function deconvolution of a nearby M 1.4 earthquake. The moment rate functions show a duration of approximately 0.2 seconds, which is expected for an event of this magnitude.

2.3 Double-Difference Wadati Method

Wadati diagram are useful to determine origin times of earthquakes and to estimate Vp/Vs ratios below the recording network. In the present study, we apply the double-difference Wadati (DDW) technique to high-accuracy P- and S-wave differential travel times derived from subsample waveform cross correlation to image fluid saturation in the subsurface based on Vp/Vs-ratio. The recently developed technique has been applied to estimate temporal changes of fluid distribution in fault zones (Lin and Shearer, 2007, 2009) and in volcanic regions (Dahm and Fischer, 2013) but not yet in engineered geo-reservoirs. The advantage of using double-differences of P- and S-wave travel times between neighboring events is that medium effects along the common propagation paths from the events to a common station are eliminated, which results in more precise relative hypocenter locations (Waldhauser and Ellsworth, 2000) and allows to determine Vp/Vs ratio in the near source region with higher accuracy than tomographic methods.

Estimating Vp/Vs ratio from DDW requires accurate fitting techniques, since the differential travel times of the seismic waves propagating from neighboring events to a common recording station can be quite small. Therefore, we first implemented and tested a robust misfit fitting technique to estimate Vp/Vs ratio from differential, or double-difference, travel times of earthquake clusters on a Wadati diagram. The concept of the method is illustrated in Figure 11, where two events are located close to each other in a source region at far distance from the seismic recording stations. Due to the geometrical constraints the ray paths outside the source region to the recording station can be considered the same, while the separation distance between the events in the source region can be defined as δl. By differencing the P- and S-wave travel times of the seismic waves from the two events to the recording station, the effects of the medium along the propagation paths outside the source region are canceled. As a result the slope of the differential travel times, plotted on a Wadati diagram, yields an estimate for the Vp/Vs ratio in the source region of the two events. We refer to the study by Line and Shearer (2007) for an explanation of the details of DDW.

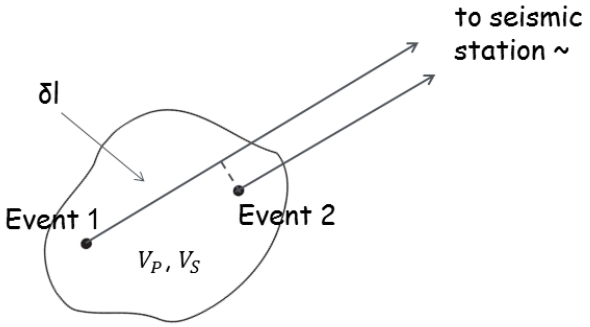

Figure 11: Two events located close to each other in the source region, separated by the distance δl. If the recording station is located at far distance from the two events, the ray paths from the source region to the seismic station can be considered common.

In order to appraise robust fitting techniques, a numerical study was conducted, where a cluster of earthquakes was assumed to be locate below the Prati-32 injection well. Theoretical travel times were calculated from each event to each sensor in the 34-station network, assuming a constant Vp/Vs ratio of 1.73 for the volume of The Geysers below the surface station. The absolute travel times were subsequently used to derive differential P- and S-wave travel times for neighboring pairs of events. The travel times in real field applications are typically contaminated by noise from errors related to the determination of phase arrivals. Therefore, we added Gaussian distributed noise with zero mean and 10 ms standard deviation to both P- and S-wave differential arrival times. The 10 ms standard deviation represents a relative large error for seismic data recorded at The Geysers of up one quarter of a wavelength. In order to simulate outliners in real data, we added uniformly distributed noise with a standard deviation of 0.3 s to 5% of the differential P-wave travel time data. The resulting differential travel times, plotted on a Wadati diagram are displayed in Figure 12a. It can be seen how the cloud of differential travel times is spread out due to the addition of noise in the data. When trying to employ linear least squares fitting techniques it is important to consider which data points are affected by noise. In the present case, Gaussian distributed noise was added to both differential P- and S-wave arrival time, while uniformly distributed noise was added as outliers to the differential P-wave arrival times. Often times least squares fitting of (x,y) data points is based on the assumption that only the x-data points are affected by errors, while the y-data points are assumed error free. When such assumption is made in the current example and a straight line is fitted to the data in Figure 12a using linear least squares, the resulting slope yields a value of 0.894 (red line in Figure 12a. The problem in this example is that the fitting is greatly affected by the outliers in the differential P-wave travel times and by the errors that are present in both differential P-wave (x-values) and differential S-wave (y-values) travel time data. The estimate of the slope improves, when errors in both variables are assumed during the least squares fitting process. However, the resulting slope with a value of 1.411 is still far off the true value of 1.732 (blue line in Figure 12a. In cases where data points may be affected by errors in both variables in addition to large outliers, as in the present example, a different fitting procedure is necessary. In such cases, the principle of least absolute deviations is employed, which minimized the sum of linear deviations, rather than its square as in least squares fitting. The technique, also referred to as median fitting, is based on the underlying principle that the median of a set of numbers is also that value which minimizes the sum of the absolute deviations. We applied median fitting to the dataset in Figure 12a, which resulted in fit with a slope of 1.520 (green line in Figure 12a). While this estimate is better than the ones resulting from linear least squares fitting, the value still underestimates the underlying Vp/Vs ratio of 1.732.

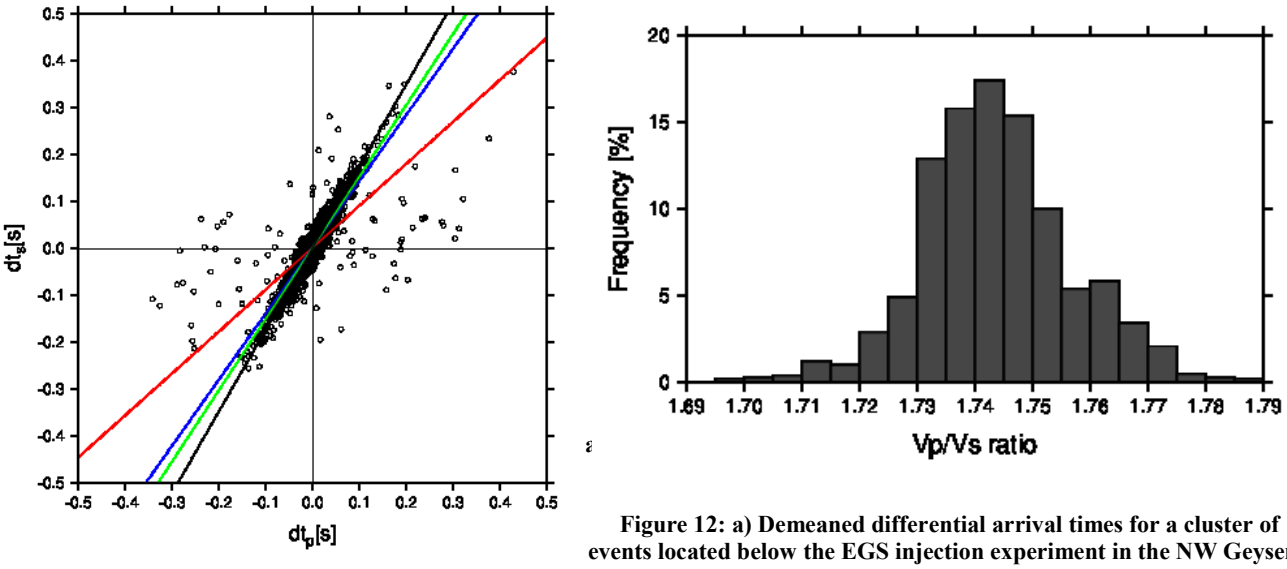

Figure 12: a) Demeaned differential arrival times for a cluster of events located below the EGS injection experiment in the NW Geysers. The data have been randomized by Gaussian and uniformly distributed noise. Red line: slope of 0.894, blue line: slope of 1.411, green line: slope of 1.520, black line: slope of 1.743. b) Frequency distribution of Vp/Vs ratio estimates from bootstrapping the data in a).

The numerical experiment reveals that in cased were errors of different magnitude are present in the data, typical fitting approaches based on minimizing either the sum of linear deviations or the sum of squared deviations is not applicable. The fitting of seismic travel time data is such a situation as shown in the example above. In this situation, a more robust fitting technique is required. Therefore, we implemented and tested the robust L1-L2 norm, which is based on different minimization depending on the error in the data (Huber, 1973). For data where the misfit is less than a specified distance the L2 norm is applied while for larger distances the L1 norm is utilized. Distance in this case is perpendicular to the fitted slope, to account for error in differential P- and S-wave arrival times. In the current case, we apply a grid search method to fit lines of varying slopes through the data cloud in Figure 12a. The fitting technique is refined by eliminating data points with the largest distance from the fitted line. The data points beyond a predefined distance from the line will be fitted by the L1 norm, while the remaining data will be fitted by the L2 norm. Using this technique, the fitting resulted in a slope of 1.743 (black line in Figure 12a, which is only 0.6% off the true Vp/Vs ratio of 1.732. We applied bootstrapping to the data points in Figure 12a to appraise the uncertainty in the estimates of the slope and obtained the frequency distribution of Vp/Vs ratios in Figure 12b. The standard deviation resulting from the bootstrapping technique is $\sigma = 0.023$, which indicates that the estimate of 1,743 from the robust L1-L2 norm constitutes a statistically significant fit to the true Vp/VS ratio of 1.732.

This example shows the robustness of the L1-L2 norm in cases where data are contaminated by errors in both variables including outliers in some of the data. The uncertainty added to the data points, including Gaussian distributed noise with zero mean and 10 ms standard deviation to both P- and S-wave differential arrival times and uniformly distributed noise with a standard deviation of 0.3 s to 5% of the differential P-wave travel time data, constitutes a maximum limit to the error that can be expected in the seismic data recorded at The Geysers. Therefore this fitting technique appears best suited to estimate Vp/Vs ratio from Wadati diagrams for earthquakes related to the EGS experiment at The Geysers geothermal reservoir.

Waveform cross correlation can be used to estimate the travel time differences for P- and S-waves with high accuracy and this technique was investigated by Lin and Shearer (2007). In the following example, however, we utilize a methodology suggested by Taira and Kato (2013), which estimates travel time differences by combining waveform cross correlation with a multiple sliding window approach that promises more stable time estimates. The method is particularly suited for situations where S-wave arrival times are not available, either due to poor signal-to-noise ratio or when the onset of the S-wave arrival is covered by signals from the P-wave coda, which makes windowing for waveform cross correlation techniques challenging. In the present case, the technique by Taira and Kato (2013) was applied to a cluster of events in The Geysers geothermal reservoir. The map in Figure 13a displays a topographical map of The Geysers including the location of the earthquake cluster (white circle), while the red triangles denote those stations of the network that recorded the individual events in the cluster. The recorded waveforms for each event-pair were analyzed using a sliding window approach to estimate the correlation between the traces. Differential travel time were subsequently derived by fitting a step-function to the delay time between P and S-wave phases. The resulting cluster of demeaned differential travel times is presented in Figure 13b, where the same fitting techniques, described in the last section, were applied. Applying a linear least squares fitting approach, while considering uncertainties in the P-wave data only, yields a fit with an estimate of 0.90, as presented by the red line in Figure 13b. In contrast, linear least squares fitting assuming uncertainties in P- and S-wave data yields a fit of 1.22 (blue line in Figure 13b). When median fitting is applied to the data the resulting fit is 1.23 (green line in Figure 13b). Because the fits from linear least squares and median fitting are similar, the two lines are practically superimposed and difficult to distinguish in Figure 13b. Finally, when the robust L1-L2 norm is applied to fit the data the resulting slope is 1.54. Bootstrapping the data points in Figure 13b yields a standard deviation of $\sigma = 0.05$. The estimate of 1.54 for the Vp/Vs ratio in the south-central Geysers may appear low compared to a "typical" value of 1.732 for crustal rocks. However, past studies on Vp/VS ratio have reported that low Vp/VS ratios are typically relate to gaseous fluids, while high Vp/Vs ratios are related to liquid fluids in the subsurface (Julian et al., 1996; Gunasekera et al., 2003, Gritto et al, 2004, Gritto and

Jarpe, 2013, 2014). The Geysers is a steam dominated reservoir with ubiquitous surface manifestations of the presence of steam. In Figure 13a the station FUM just east of the white circle is named after the Fumarole steam field where steam is venting from the soil. Additionally, the black line south of the white circle is the surface trace of the Big Sulfur Creek Fault. The name is derived from sulfur deposits found on rocks along the creek bed. Gritto et al. (2013) reported low Vp/Vs ratios in this part of The Geysers from seismic tomography studies. Therefore, it is reasonable to assume that the low Vp/Vs ratio estimate of 1.54 for the source region of the earthquake cluster in is another manifestation of the presence of steam in this part of the reservoir.

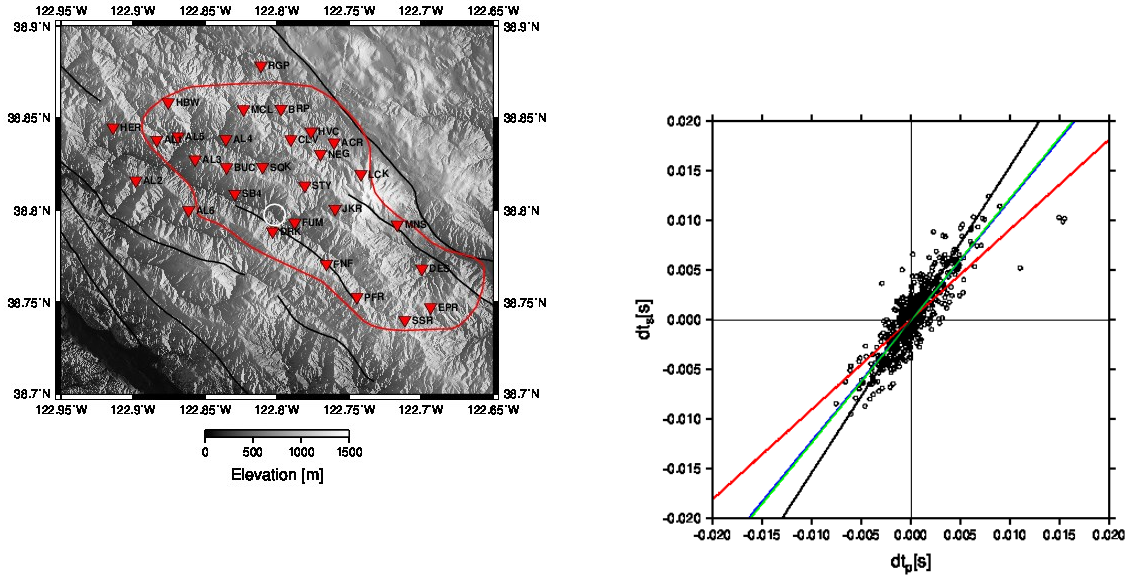

a) **b)**

Figure 13: a) Topographical map of The Geysers with the location of the earthquake cluster (white circle) and the geophone stations that recorded the events. b) Demeaned differential arrival times for the cluster of events in a). Red line: slope of 0.90, blue line: slope of 1.22, green line: slope of 1.23, black line: slope of 1.54. The blue and green lines are practically superimposed due to their similar fits.

2.4 Conclusions

A catalog of seismic moment tensor of micro earthquakes has been developed in The Geysers associated with the Prati-32 EGS stimulation experiment. The results for more than 80 M>1.0 earthquakes reveals that there are two dominant populations, one strike-slip and the other normal. This is consistent with prior results (e.g., Guilhem et al., 2014; Boyd et al., 2015). Some of the solutions show large non-double-couple terms and full moment tensor solution suggest a volume increase component. Preliminary analysis of first-motion and waveforms indicates that the volume increase component maybe real, however, more analysis is needed to confirm this observation. The search for suitable target and empirical Green's function event pairs thus far has resulted in the determination of seismic moment rate functions for five events. The moment rate functions have been inverted for finite-source parameters, and the area scaling has been compared to a published scaling relationship. The results indicate that the finite-source parameters are mostly consistent with the published relationship, however, The Geysers events tend to have more compact rupture areas than predicted by the equation. As finite-source parameters for more earthquakes are obtained they will be used to calibrate the magnitude rupture-area scaling relationship for The Geysers. The seismic moment tensor catalog, the relationships between catalog magnitude and moment magnitude and the source-area scaling relationship will subsequently be used to estimate the coseismic fracture density of the EGS swarm. The moment tensor catalog will also be used to invert for the in situ state of stress and to investigate possible temporal variations during the stimulation experiment.

We applied the double-difference Wadati (DDW) technique to high-accuracy P- and S-wave differential travel times derived from subsample waveform cross correlation to image fluid saturation in the subsurface based on Vp/Vs-ratio. In order to appraise robust fitting techniques, a numerical study was conducted, where a cluster of earthquakes was assumed to be located below the Prati-32 injection well. Theoretical travel times were calculated for a constant Vp/Vs ratio and errors in the data modeled by Gaussian distributed noise and by outliers in P-wave travel time. Several fitting techniques were applied to demonstrate the care must be taken when fitting data with uncertainties of varying magnitude. In the case of seismic travel time data, the robust L1-L2 norm appears suitable to deliver accurate estimates of linear fits with reasonable uncertainties. The application of waveform cross correlation combined with a multiple sliding window approach (Taira and Kato, 2013) to seismic waveform data from an earthquake cluster in the south-central Geysers yielded a low estimate of Vp/Vs (1.54) that might be indicative of the presence of steam in this part of the reservoir.

REFERENCES

Boyd, O. S., D. S. Dreger, V. H. Lai, and R. Gritto (2015). A systematic analysis of seismic moment tensor at The Geysers geothermal field, California, *Bull. Seism. Soc. Am.* **105**, 2969-2986, doi:10.1785/0120140285.

Dahm, T., and Fischer, T. (2013), Velocity ratio variations in the source region of earthquake swarms in NW Bohemia obtained from arrival time double-differences. *Geoph.. J. Int*., doi: 10.1093/gji/ggt410.

Dreger, D., R. Nadeau and A. Chung (2007), Repeating earthquake finite-source models: Strong asperities revealed on the San Andreas Fault, *Geophys. Res. Lett.,* **34**, L23302, doi:10.1029/2007GL031353.

Ford, S. R., D. S. Dreger and W. R. Walter (2010). Network sensitivity solutions for regional moment tensor inversions, *Bull. Seism. Soc. Am.*, **100**, 1962-1970.

Gritto, R.; Romero, A. E., Daley, T. M., (2004), Results of a VSP Experiment at the Resurgent Dome, Long Valley Caldera, California, *Geophys. Res. Lett.*, **31**, No. 6, L06603, 10.1029/2004GL019451.

Gritto, R., Yoo, S.H., Jarpe, S., (2013), Three-dimensional seismic tomography at The Geysers geothermal field, CA, USA. *38th Workshop on Geothermal Reservoir Engineering*, February 11–13, SGP-TR-198,Stanford University, Stanford, CA, pp. 1–12.

Gritto, R. and S.P. Jarpe, (2014), Temporal variations of Vp/Vs-ratio at The Geysers geothermal field, USA, *Geothermics*, http://dx.doi.org/10.1016/j.geothermics.2014.01.012.

Guilhem, A., L. Hutchings, D.S. Dreger and L.R. Johnson (2014), Moment tensor inversions of M ~ 3 earthquakes in The Geysers geothermal fields, California, *J. Geophys. Res.*, 10.1002/2013JB010271.

Gunasekera, R.C., Foulger, G.R., Julian, B.R., (2003), Reservoir depletion at The Geysers geothermal area, California, shown by four-dimensional seismic tomography. *J. Geophys. Res.,* **108**, 2134, http://dx.doi.org/10.1029/2001JB000638.

Herrmann, R. B. (2013). Computer programs in seismology: An evolving tool for instruction and research, *Seism. Res. Lett*., **84**, 1081-1088, doi:10.1785/022011096.

Huber, P. J. (1973). Robust regression: asymptotics, conjectures and monte carlo, Ann. Statist., **1**, 799–821.

Julian B.R., A. Ross, G.R. Foulger, and J.R. Evans (1996), Three-dimensional seismic image of a geothermal reservoir: The Geysers, California, *Geophys. Res. Lett*., **23**, doi:10.1029/96GL03321.

Lin, G., Shearer, P., (2007), Estimating local Vp/Vs ratios with similar earthquake 397 cluster, *Bull. Seism. Am.*, **97** (2), 379–388, 398, http://dx.doi.org/10.1785/0120060115.

Lin, G., and Shearer, P.M., (2009), Evidence for water-filled cracks in earthquake source regions: *Geophys. Res. Lett.*, **36**, L17315, doi:10.1029/2009GL039098.

Majer, E.L., Peterson, J.E., (2007) Impact of injection on seismicity at The Geysers, California geothermal field, *Int. J. Rock Mech. Min. Sci.*, **44**, 1079–1090.

Minson, S.E. and D.S. Dreger (2008), Stable inversions for complete moment tensor, *Geophys. J. Int.* **174**, 585-592, doi: 10.1111/j.1365-246X.2008.03797.x.

Mori, J. (1993), Fault plane determination for three small earthquakes along the San Jacinto fault, California: Search for cross faults, *J. Geophys. Res*., **98**, 17,711– 17,722.

Nayak, A. and D. S. Dreger (2015). Source-type-specific inversion of moment tensors, *Bull. Seism. Soc. Am.*, **105**, 2987-3000, doi: 10.1785/0120140334.

Ripperger, J., and P. M. Mai (2004), Fast computation of static stress changes on 2D faults from final slip distributions, *Geophys. Res. Lett*., **31**(18), L18610, doi:10.1029/2004GL020594.

Waldhauser, F. and W.L. Ellsworth, (2000), A double-difference earthquake location algorithm: Method and application to the Northern Hayward Fault, California: *Bull. Seism. Am.*, **90**, 1353-1368.

Wells, D. L. and K. J. Coppersmith (1994), New empirical relationships among magnitude, rupture length, rupture width, rupture area and surface displacement, *Bull. Seism. Soc. Am*., **84**, No. 4, 974-1002.